Mode control and loss compensation of propagating surface plasmons

Zhili Jia[a], Deng Pan[a], Hong Wei[a], Hongxing Xu*[a,b]

[a] Institute of Physics, Chinese Academy of Sciences, and Beijing National Laboratory for Condensed Matter Physics, Beijing 100190, China
[b]Center for Nanoscience and Nanotechnology, and School of Physics and Technology, Wuhan University, Wuhan 430072, China

*hxxu@iphy.ac.cn

ABSTRACT

Plasmonic devices can be used to construct nanophotonic circuits and are very promising candidates for next-generation information technology. The functions of plasmonic circuits rely on the rigorous control of plasmon modes. Two different methods were proposed to control the propagation of surface plasmons (SPs) supported by Ag nanowires (NWs). The first one is modulating the beat period of the near-field distribution pattern, which can be realized by depositing Al_2O_3 layer or changing the refractive index of surrounding medium. The beat period increasing by 90 nm per nanometer of Al_2O_3 coating or by 16 μm per refractive index unit was obtained in experiments. The second one is introducing local structural symmetry breaking to realize mode conversion of SPs. Three typical structures including NW-nanoparticle (NP) structure, branched NW and bent NW were used to investigate the mode conversion. It's revealed that the mode conversion is a scattering induced process. The lossy characteristic of SPs at optical frequencies typically limits the propagation length and hinders the further development of integrated plasmonic circuits. CdSe nanobelt/Al_2O_3/Ag film hybrid plasmonic waveguide was proposed to compensate the loss of SPs by using an optical pump-probe technique. Compared to the measured internal gain, the propagation loss was almost fully compensated for the TM mode. These results for mode control and loss compensation of propagating SPs are important for constructing functional nanophotonic circuits.

Keywords: Surface plasmons, nanowire, near field distribution, mode conversion, routing, switch, loss compensation, nanophotonic circuitry

1. INTRODUCTION

Surface plasmons (SPs) have intrigued intensive researches in recent years. The SPs are electromagnetic waves supported on metal nanostructure surfaces, which show strong confinement of electromagnetic field even beyond the diffraction limit of light. Many kinds of metal nanostructures used as plasmonic waveguides have been investigated, such as strips[1, 2], nanowires[3, 4], nanogrooves[5, 6], and so on. Silver nanowires synthesized by chemical method are known to be efficient plasmonic waveguides due to their high field confinement as well as low waveguiding losses[7]. B Based on the unique properties of NW SPs, the NW-based waveguides can construct the basic functional units of nanophotonic circuits. For example, sensor[8], polarization rotator[9], resonator[10], router[11] and logic gates[12, 13] have been proposed and implemented.

There are two basic problems to be considered in building plasmonic circuits. The first one is controlling the propagation of SPs in the circuits and the second one is compensating the material loss of SPs induced by the metal. The control to the SP propagation includes controlling the mode distribution and conversion between different SP modes. The mode distribution as well as the dispersion relations and resonance energies of SPs can be influenced by the refractive index of the surrounding medium[14]. Therefore, Changing the dielectric environment provides a method to control the mode distribution of propagating SPs. Symmetry breaking in individual nanoparticle can modify the selection rules for the interaction of plasmon modes[15]. Symmetry-broken nanoantennas can control spatial and spectral distributions of light field at the nanoscale[16]. Inspired by this, the mode conversion for controlling SP propagation can be realized by introducing the structural symmetry breaking into the plasmonic waveguide structures. As the SPs suffer loss in metal nanostructure, the SP signal is damped during propagation. The loss of the metal will hinder the integration of plasmonic

Plasmonics: Metallic Nanostructures and Their Optical Properties XII, edited by Allan D. Boardman, Proc. of SPIE Vol. 9163, 91630O · © 2014 SPIE
CCC code: 0277-786X/14/$18 · doi: 10.1117/12.2062293

devices into nanophotonic circuits. Some schemes have been proposed to compensate the loss of SPs using gain medium such as fluorescent molecules[17, 18], organic materials[19], and quantum dots (QDs)[20]. However, mode confinement cannot guarantee when loss-compensation is obtained. Semiconductor-insulator-metal hybrid plasmonic waveguide has low propagation loss and better sub-wavelength mode confinement[21]. Furthermore, the semiconductor material can provide the gain for loss compensation. Thus, this kind hybrid plasmonic waveguide provides an ideal platform for investigating the compensation of SP loss.

In this paper, we will introduce how to realize mode control and loss compensation of propagating SPs. The beat periods of the near-field distribution pattern are largely modulated by depositing Al_2O_3 layer or changing the refractive index of surrounding medium. Mode conversions of SPs are achieved in symmetry broken structures. Hybrid plasmonic waveguide of CdSe nanobelt/Al_2O_3/Ag film is demonstrated to compensate the loss of SPs.

2. MODE CONTROL OF PROPAGATING SURFACE PLASMONS

2.1 Controlling the beat periods of propagating surface plasmons

An extremely large tunability of beat periods of propagating SPs on Ag NWs has been observed using the QD fluorescence imaging technique[22]. The cross-section of the NW structure supporting the SPs is shown in Fig. 1a. Here Ag NWs with pentagonal cross-section are deposited on a glass substrate and then coated with Al_2O_3 layers with different thicknesses. A layer of quantum dots (QDs) is spin-coated on the sample subsequently. Finally, the structures are surrounded by a medium. As shown in Fig. 1b, the SPs propagating on the Ag NW are excited by focusing laser light of 633 nm wavelength at one end of the NW. The coated QDs are excited by the propagating SPs and the fluorescence is recorded by a CCD camera after filtering the laser light, which can provide the field distribution of SPs on the NW. The excitation and collection are performed by the same objective. In the scanning electron microscope (SEM) image in Fig. 1c, the Al_2O_3 layers of different thickness can be seen clearly.

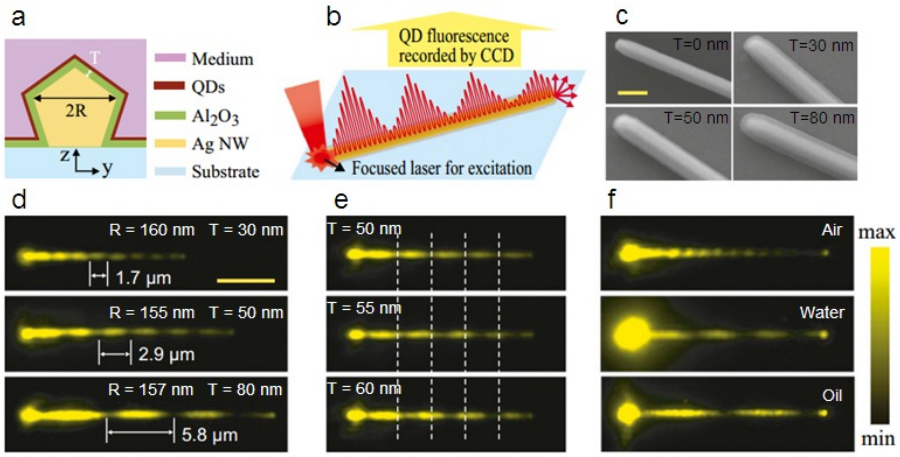

Figure 1. (a) Schematic cross-section of the sample. (b) Schematic illustration of quantum dots (QDs) fluorescence imaging technique. (c) SEM images of Ag NWs coated with Al_2O_3 layers of different thickness T. (d) QD emission images under excitation at the left end of the NWs with Al_2O_3 coating of different T. (e) QD emission images for a 162 nm radius NW with Al_2O_3 coating of different T. (f) QD emission images for a 155-nm radius NW coated with 15 nm of Al_2O_3, measured in different dielectric environments.

The experimental results for the fluorescence imaging of SPs on the Ag NWs are shown in Fig. 1d-f. In all these results, the SPs exhibit periodic distributions which result from the beating of different modes on the NWs. The period Λ of the field distribution sensitively depends on the structural geometry and materials. As shown in Fig. 1d, for NWs of similar radius R, the period Λ of near field increases dramatically with the thickness T of the Al_2O_3 layer. The sensitive dependence of the period Λ on the thickness T is further illustrated by the experimental result in Fig. 1e. For the same 162 nm radius NW, the near-field beat period is 2.9 μm when the thickness of Al_2O_3 layer is 50 nm. The beat period increases to 3.3 μm when 5 nm Al_2O_3 layer is added and to 3.8 μm with an additional 5 nm Al_2O_3 layer. It is found that

the beat period of the near-field distribution increases 90 nm when the coating thickness is increased 1 nm. Furthermore, the increment of each period can induce obvious shift of the last period as $N \cdot \Delta\Lambda$, where N is the number of total periods. Immersing the samples in medium with higher refractive index n can also increase the beat period, as demonstrated in Fig. 1f. Here the media surrounding the NW are air, water and oil, with refractive indexes of 1.00, 1.33 and 1.51, respectively. The corresponding beat period is 1.3 μm in air, 4.4 μm in water and 7.2 μm in oil. The value of $\Delta\Lambda/\Delta n$ is 9.4 μm/RIU from air to water and 16 μm/RIU from water to oil, where RIU is refractive index unit. Due to the accumulation effect, the corresponding sensitivity is 3×9.4 μm/RIU = 28.2 μm/RIU from air to water and 2×16 μm/RIU = 32 μm/RIU from water to oil, respectively. Therefore, much higher sensitivity can be obtained if the Ag NW is long enough.

The experimentally observed period of the SP field results from the beating between different SP modes on the NW. Figure 2a shows three lowest-order SP modes (H_0, H_1, and H_2) for a coated NW (R=110 nm, T=80 nm) on a glass substrate. From Fig. 2bi-bv, we can see that H_0 and H_2 modes are excited and interfere with each other to form the periodic field distribution. The beat period can be calculated by using the equation $\Lambda = 2\pi/\mathrm{Re}(\Delta k_{//})$, where $\Delta k_{//}$ is the difference of the propagation constant of the H_0 and H_2 modes. The beat period of coated NWs depends on the NW radius R and coating thickness T. As shown in Fig. 2c, for thick coating (T=80 and 100 nm) the period Λ increases monotonically with the increasing of R. This results from the decrease of $\mathrm{Re}(\Delta k_{//})$ with increasing R as shown in Fig. 2d. For thin coating (T≤50 nm), the increase of Λ reaches saturation for R greater than about 125 nm, when H_2 becomes leaky mode. The dependence of the period on the thickness T is shown by the experimental and simulation results in Fig. 2e and 2f. For certain R, Λ increases with the increase of T and then gets to saturation, which accords with the trend of $\mathrm{Re}(\Delta k_{//})$ obtained from Fig. 2f.

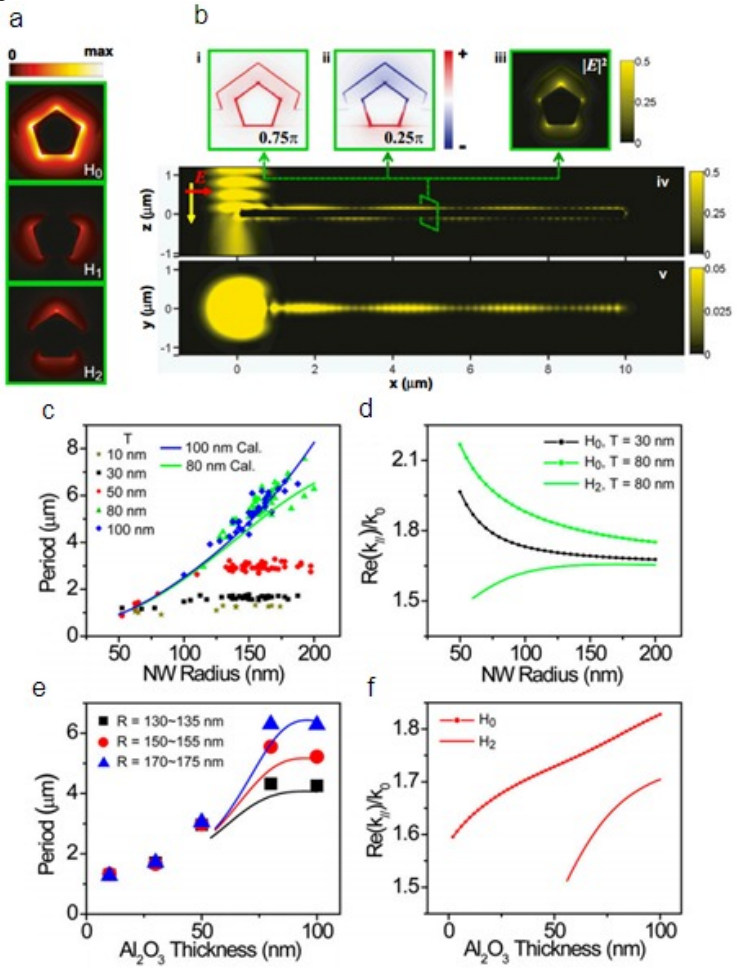

Figure 2. (a) Power distribution of three lowest-order modes on supported NW. (bi, bii) Charge plots with different initial phase; (biii–bv) Electric field intensity distribution on different cross-section of the Ag NW. (c-f) The beat period (c, e) and the $\mathrm{Re}(k_{//})$ of the H_0 and H_2 mode (d, f) as a function of NW radius (c, d) and Al_2O_3 coating thickness (e, f). In c and e, the dots are experimental data, and the lines are calculated data.

2.2 Mode conversion of propagating surface plasmons

Mode conversion of propagating SPs in plasmonic NWs with local structural symmetry breaking has been proved experimentally and theoretically[23]. Three typical kinds of NW-based structures used for mode conversion, including NW-nanoparticle (NP) structure, branched NW and bent NW, are schematically shown in Fig. 3a. The SPs on the NW are excited by laser light of 633 nm wavelength with polarization parallel to the main Ag NW. The propagation of the SPs on these three kinds of structures are experimentally revealed by the fluorescence imaging technique used in section 2.1, with the results shown in Fig. 3b-3d. For the excitation with parallel polarization, only the fundamental TM_0 mode can be excited, which can be verified by the symmetric field distribution of the generated SPs on the forepart of the structures. More importantly, it is clear that the field distributions are changed from symmetric shapes to zigzag shapes after the symmetry-broken regions. This phenomenon is reproduced in the simulations, and the results are shown in Fig. 3e. The change in the symmetry of the SP field implies a mode-conversion process. The zigzag shapes of SPs observed in the experiments and simulations are the result of coherent superposition of the fundamental TM_0 mode and a higher order HE_1 mode shown in Fig. 3f and 3g. The period of this shape is also determined by the difference of the propagation constant of the two modes, similar to the mode beating discussed in section 2.1. Therefore after the symmetry-broken regions, some power of the directly generated TM_0 mode is converted into HE_1 mode.

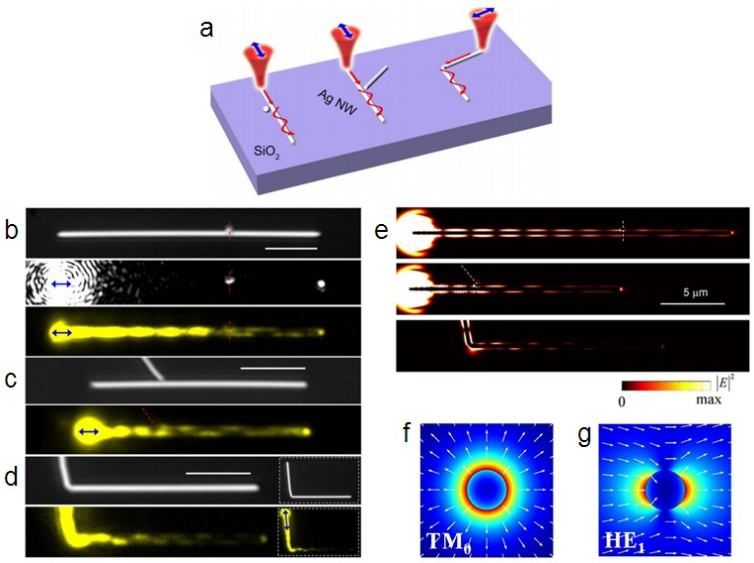

Figure 3. (a) Diagram for three kinds of symmetry-broken Ag NW-based structures. (b-d) Experimental results of NW–NP structure (b), branched NW (c), and bent NW (d). Top: white light optical images. Bottom: QD fluorescence images. The middle image in (b) is the corresponding scattering image. The scale bars are 5 μm. The radius of the NWs is about 150 nm. (e) Simulation results of field intensity distributions for the mode conversions in the three kinds of structures. Top: NW-NP structure. Middle: branched NW. Bottom: bent NW. (f, g) Electric field distribution of two lowest order modes (TM_0 and HE_1) in a Ag NW with a radius of 60 nm at the wavelength of 633 nm.

The NW-NP structure in uniform dielectric environment is chosen for illustrating the mode conversion mechanism. Figure 4a shows the schematics for the conversion processes in the NW-NP structure. In this structure, a wave of TM_0 mode with its original wave front $T_{in}(R)$ propagates along the Ag NW with its final wave front as $T_{out}(R)$, where R represents the position vector in the plane perpendicular to the NW. The symmetry of structure in x direction is broken by the NP. As a result, the $T_{out}(R)$ is asymmetric and will bring a nonzero component of HE_1 mode from the mathematical perspective. Intuitively, in this structure the nanoparticle plays a role in scattering the power of light. There are two scattering processes contributing to mode conversion. Process I corresponds to the scattering of power coupling back into NW. Process II corresponds to the scattering of power into free space. In Fig. 4b, the drops in the transmittance

spectra result from power scattering into the free space due to the resonant gap modes. The resonant modes red-shift with the decrease of h. As shown in Fig. 4c, η_{01} is the efficiency of conversion from TM_0 mode to HE_1 mode, and η_{00} is the transmission efficiency for the remaining TM_0 mode for h=3 nm.

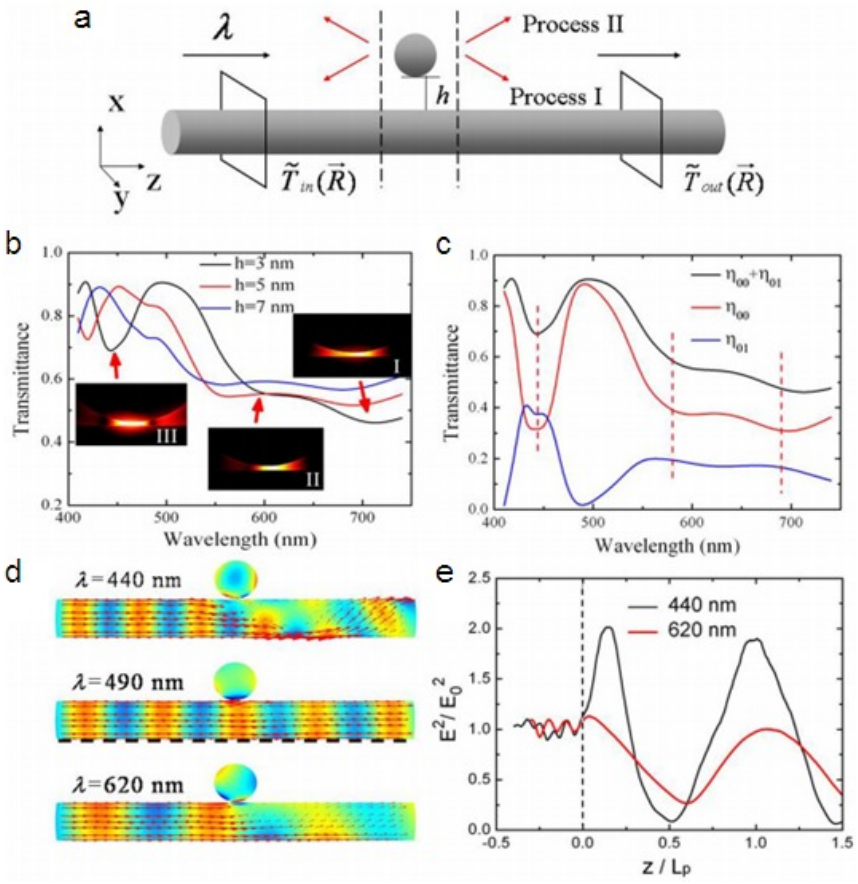

Figure 4. Mechanism of the mode conversion in the NW-NP structure. (a) Schematic illustration of the mode conversion in NW-NP structure. (b) Total transmittance spectra for different separation h. Insets: the electric field distributions (|E|) of the resonant gap modes corresponding to the drops in the spectrum for h=3 nm. (c) Black: the total transmittance spectrum. Red: the transmittance spectra of the remaining TM0 mode. Blue: efficiency of mode conversion from TM_0 mode to HE_1 mode. h=3 nm. (d) Distributions of power flow (arrows) and instant surface charges (color coordinate) for three typical wavelengths. (e) Electric field intensity distribution at the bottom of the NW for different wavelengths.

From the distributions of power flow and instant surface charges in Fig. 4d, the mode conversion can be interpreted. Here, three different wavelengths of laser are used to excite SPs on the Ag NW. The gap between NW and NP is on-resonant for wavelength of 440 nm. The highly localized field in the nanogap can act as a point source to excite the NW SPs in a high efficiency. The power flow and the wave front become asymmetric after the nanoparticle. The power flow on the top side of the NW is scattered by the particle and flows to the bottom side. For this case, Process I is dominant and the scattering is stronger. The nanogap is off-resonant for wavelength of 490 nm and 620 nm. When the wavelength is 490 nm, Process I is dominant and the scattering is weaker. Therefore, the conversion efficiency is lower. When the wavelength is 620 nm, Process II is dominant and the scattering is stronger. The power flow on the top side of the NW is scattered by the particle without flowing to the bottom side. For wavelength of 440 nm and 620 nm, TM_0 mode can convert to HE_1 mode. The power flows on the NW during the scattering for on-resonance (440 nm) and off-resonance (620 nm) discussed above are further quantitatively illustrated in Fig. 4e. The distributions of electric field intensity on the line at the bottom of the NW (marked by the black dash line in the middle panel of Fig. 4d) for 440 nm and 620 nm are shown. For 440 nm, the intensity of the electric field is doubled after the particle (z>0), which means almost all the power on the upper side of the NW is scattered to the bottom. In contrast, for 620 nm the electric field intensity at the

same position is hardly changed compared with the field intensity before the particle ($z<0$), that is, no large scattering power is directed to the bottom. In both situations, the scattering introduces asymmetric wave front with new component of HE_1 mode, and zigzag distributions occur for the following propagation. The mode conversion in Ag NW-NP structure results from scattering induced processes, and the above discussions can also be applied to the branched NW structure.

2.3 Application of mode control

Mode control of propagating SPs can be used in designing NW-based plasmonic devices. Figure 5 shows the application of mode control for routing of SP signals in Ag NW networks. Figure 5a shows a branched structure coated with 30 nm Al_2O_3 layer excited by supercontinuum light. The polarization of the incident light is parallel to the main NW. Wavelength responses of the structure are investigated by the analysis of emission spectra from the terminals A and B. For the original structure, emission spectra from the terminals A and B are similar. The dominating wavelengths of light transmitted to terminal A are around 633 and 820 nm. After depositing an additional 5 nm of Al_2O_3 (red lines), the transmission around 633 nm increases and the transmission around 800 nm is unaffected for terminal A. For terminal B, the intensity of both the two wavelengths increases. When adding an additional 5 nm of Al_2O_3 (blue lines), transmission around 800 nm and 633 nm decrease obviously for terminal A and terminal B, respectively. From the QD emission images shown in Fig. 5c, we can see that the field intensity at the junction position of the right branch becomes stronger after depositing 5 nm of Al_2O_3. Therefore, more SP signal is routed to this terminal. From the above analysis, it is found that the routing of light to different terminals of the device can be controlled by changing the thickness of Al_2O_3 layer.

The mode conversion effect in the branched-NW-NP structure can also be used for designing the routing of SPs in nanowire networks. Figure 5d and 5e show the field intensity distributions of the structure for different positions of the nanoparticle on the main NW. As can be seen, the SPs can be routed to different branch wires by just tuning the position of the nanoparticle. The power switching between the two output branches make the structure function as a single-pole double-throw switch.

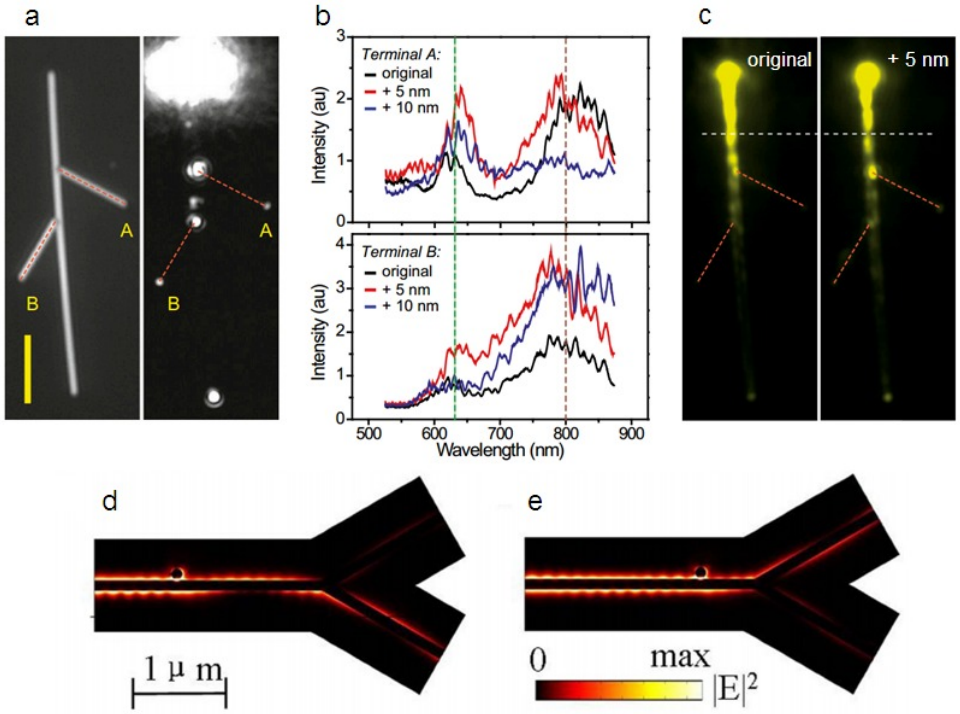

Figure 5. Application of mode control of propagating SPs. (a) White light optical image (left) and scattering optical image of a branched NW structure excited by supercontinuum light with the polarization parallel to the main NW. (b) The emission spectra for terminals A and B. (c) The QD emission images of the branched NW structure excited by laser light of 633nm wavelength. (d, e) Nanoparticle-mediated mode conversion for a tunable switch in a branched NW.

3. LOSS COMPENSATION OF PROPAGATING SURFACE PLASMONS

The most severe problem the plasmonic waveguides confronted with is the high material loss, which is inevitably accompanied with the high confinement. The scheme to resolve this problem is using the gain material to amplify the SP signal and compensate the loss[24, 25]. Highly efficient, broadband and polarization-tunable loss compensation is achieved in CdSe nanobelt/Al_2O_3/Ag film hybrid plasmonic waveguide at room temperature by using an optical pump-probe technique[26]. The diagram of the hybrid plasmonic waveguide (CdSe nanobelt/Al_2O_3/Ag film) for loss compensation of propagating SPs is shown in Fig. 6a. The Ag film with thickness of 40 to 60 nm is thermally evaporated onto the glass substrate. The Al_2O_3 layer of 4 to 5 nm thickness is deposited subsequently on top of the Ag film by atomic layer deposition (ALD) method at 200 ^oC. Finally, CdSe nanobelts (NBs) prepared by chemical vapor deposition (CVD) are put on the top of the Al_2O_3 layer. The CdSe NB used here has a rectangle cross section. In the experiment, a supercontinuum source (10 MHz repetition rate, 72 picosecond pulse width) is used to provide both pump and probe light. The probe signal and pump light on the waveguide can overlap in both space and time by adjusting the optical delay line in the light path. In such a case, the amplification of probe signal through stimulated emission takes place. Figure 6b shows optical images obtained by using a band pass filter (730 ± 5 nm). It is obvious that the intensity of output signal when both pump and probe laser are present (III) is stronger than the situation when there is only probe (I) or pump (II) light. This indicates that the probe signal is amplified when the NB is excited by the pump light. As shown in Fig. 6c, emission spectra can be obtained from the output end of the waveguide marked by white dashed circles in Fig. 6b. It can be seen from the spectra that all wavelengths in the probe signal, spanning over 10 nm, are amplified, demonstrating the broadband nature of the loss compensation scheme.

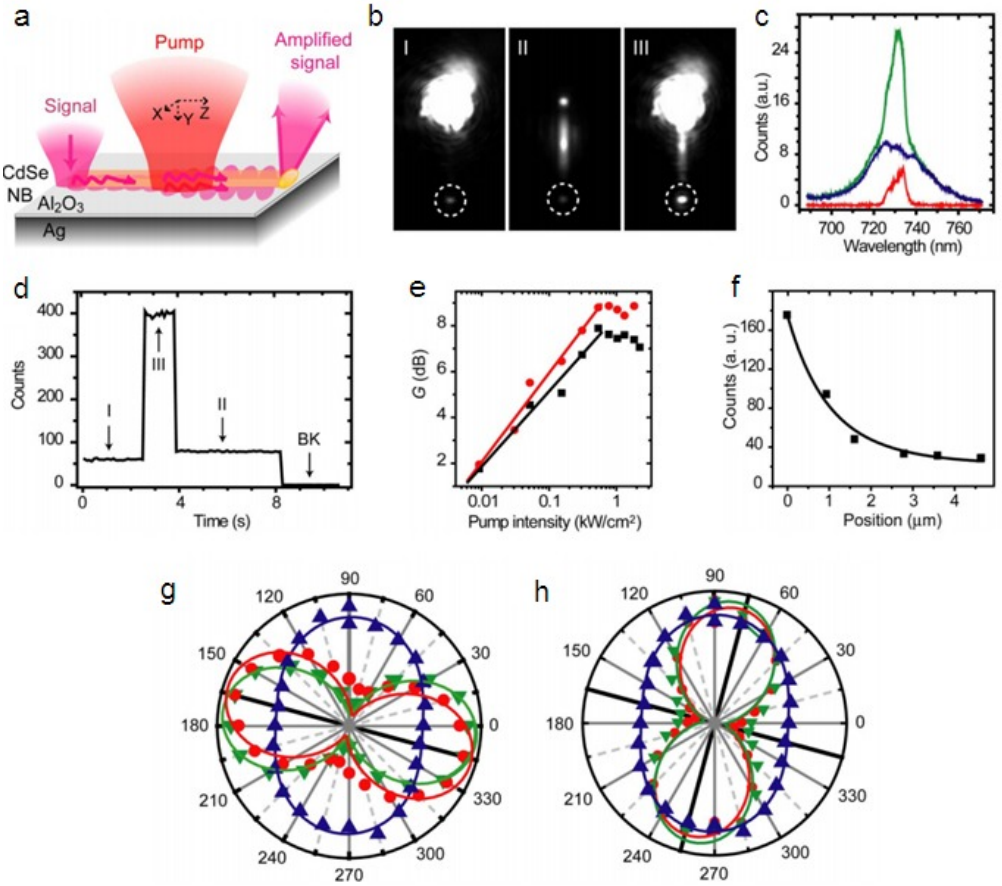

Figure 6. (a) Diagram of the hybrid plasmonic waveguide (CdSe NB/Al_2O_3/Ag film) for loss compensation of propagating SPs. (b) Optical image for only probe signal (I), photoluminescence (PL) with only pump light (II), and both pump and probe light are present (III). (c) Emission spectra obtained from the output end of the waveguide. Red, blue and green curves represent the probe signal, PL, and total output, respectively. (d) Time trace obtained from the area marked by dashed circles in (b). BK represents the counts from background. (e) Gain G (dB) as a function of pump intensity. (f) Propagation loss measurement by recording the output intensity as a function of pump position. (g, h) The measured emission polarization characteristics.

From the time trace in Fig. 6d, specific intensity value can be obtained and gain can be calculated by using the following equation:

$$G(dB) = 10\log\left(\frac{I_{on} - I_{sp}}{I_{off}}\right) = 10\log(G) \quad (1)$$

where I_{on} represents the total output intensity when both probe and pump light are on, I_{sp} represents the output intensity of the fluorescence emission from only the pump light, and I_{off} represents the output intensity when only the probe is on without the pump. The gain calculated for the waveguide in Fig. 6b is 7.8 dB. In order to investigate the relationship between the gain and the pump intensity, varied pump intensity is used in the experiment and the corresponding gain is shown in Fig. 6e. The black and red dots represent the measured data when the polarization of laser light parallel (TM) and perpendicular (TE) to the waveguide, respectively. The black and red lines are corresponding logarithmic fitting results. It is found that the measured gain G (dB) follows logarithmic dependence on the pump intensity. The experimental gain data can be fit by using the equation as follows:

$$G(dB) = G_0 \ln\frac{I}{I_{tr}} \quad (2)$$

where I is the pump intensity, I_{tr} is the transparency pump intensity denoting the start of the gain. Fitting result gives I_{tr} = 2.8 W/cm^2 and G_0 =1.42 and 1.68 for the polarization of pump light parallel and perpendicular to the waveguide, respectively. When the pump intensity is high enough (>500 W/cm^2), the gain is saturated. The maximum gain for the two polarizations is 8.0 and 8.8 dB, respectively. This corresponds to internal gain coefficient of 6140 cm^{-1} and 6755 cm^{-1}, respectively.

Figure 6f gives the result of propagation loss measurement. The pump intensity is 250 W/cm^2. The measured propagation loss coefficients for the TM and TE dominant modes are 6230 cm^{-1} and 11420 cm^{-1}, respectively. Compared to the measured internal gain coefficient for each mode (6140 cm^{-1} and 6755 cm^{-1}), the propagation loss was compensated 99% and 59% for the TM mode and the TE mode, respectively. In Fig. 6g and 6h, emission polarization characteristics are given. The red, blue and green symbols represent the probe signal, spontaneous decayed SPs excited by the pump, and total output signal, respectively. Polar angle corresponds to the angle between axis of CdSe NB and polarization of incident light. As can be seen, for probe signal of both TM mode (Fig. 6g) and TE mode (Fig. 6h), the polarization of the amplified signal (green) follows the polarization of the probe signal (red).

4. CONCLUSION

In conclusion, the near-field distribution control and mode conversion of propagating SPs on Ag nanowires are realized experimentally and analyzed theoretically. The beat period of the near-field distribution pattern is modulated largely by changing the surroundings, including depositing Al_2O_3 layer or changing the refractive index of the surrounding medium. The sensitivity of the period change is 90 nm per nanometer of Al_2O_3 layer or 16 μm per refractive index unit. Mode conversion is demonstrated in NW-based structures with local structural symmetry breaking. The mode conversion effect originates from the symmetry change of wave front induced by scattering of localized modes formed at the symmetry-broken regions. Both near-field control and mode conversion can be used to manipulate the propagation of SPs in nanowire networks to realize the functions such as routing and switching. In CdSe nanobelt/Al_2O_3/Ag film hybrid plasmonic waveguide, the propagation loss was almost fully compensated for the TM mode by using an optical pump-probe technique at room temperature. Loss compensation is very important to ensure the SP signal fidelity over a longer propagation distance. Therefore, these results for mode control and loss compensation would promote the development of plasmonic nanophotonic circuitry.

ACKNOWLEDGEMENTS

This work was supported by National Natural Science Foundation of China (Grant Nos. 11134013, 11227407 and 11374012), The Ministry of Science and Technology of China (Grant Nos. 2012YQ12006005 and 2009CB930700), the "Knowledge Innovation Project" (Grant No. KJCX2-EW-W04) and the "Strategic Priority Research Program (B)" (Grant No. XDB07030100) of Chinese Academy of Sciences.

REFERENCES

[1] Weeber, J. C., Krenn, J., Dereux, A., Lamprecht, B., Lacroute, Y. and Goudonnet, J., "Near-field observation of surface plasmon polariton propagation on thin metal stripes," Phys. Rev. B 64(4), 045411 (2001).
[2] Weeber, J. C., Gonzalez, M. U., Baudrion, A. L. and Dereux, A., "Surface plasmon routing along right angle bent metal strips," Appl. Phys. Lett. 87(22), 221101 (2005).
[3] Sanders, A. W., Routenberg, D. A., Wiley, B. J., Xia, Y. N., Dufresne, E. R. and Reed, M. A., "Observation of plasmon propagation, redirection, and fan-out in silver nanowires," Nano Lett. 6(8), 1822-1826 (2006).
[4] Wei, H. and Xu, H. X., "Nanowire-based plasmonic waveguides and devices for integrated nanophotonic circuits," Nanophotonics 1(2), 155-169 (2012).
[5] Pile, D. F. P. and Gramotnev, D. K., "Channel plasmon-polariton in a triangular groove on a metal surface," Opt. Lett. 29(10), 1069-1071 (2004).
[6] Bozhevolnyi, S., Volkov, V., Devaux, E. and Ebbesen, T., "Channel Plasmon-Polariton Guiding by Subwavelength Metal Grooves," Phys. Rev. Lett. 95(4), 046802 (2005).
[7] Ditlbacher, H., Hohenau, A., Wagner, D., Kreibig, U., Rogers, M., Hofer, F., Aussenegg, F. and Krenn, J., "Silver Nanowires as Surface Plasmon Resonators," Phys. Rev. Lett. 95(25), 257403 (2005).
[8] Fang, Y. R., Wei, H., Hao, F., Nordlander, P. and Xu, H. X., "Remote-Excitation Surface-Enhanced Raman Scattering Using Propagating Ag Nanowire Plasmons," Nano Lett. 9(5), 2049-2053 (2009).
[9] Li, Z. P., Bao, K., Fang, Y. R., Huang, Y. Z., Nordlander, P. and Xu, H. X., "Correlation between Incident and Emission Polarization in Nanowire Surface Plasmon Waveguides," Nano Lett. 10(5), 1831-1835 (2010).
[10] Allione, M., Temnov, V. V., Fedutik, Y., Woggon, U. and Artemyev, M. V., "Surface plasmon mediated interference phenomena in low-Q silver nanowire cavities," Nano Lett. 8(1), 31-35 (2008).
[11] Fang, Y. R., Li, Z. P., Huang, Y. Z., Zhang, S. P., Nordlander, P., Halas, N. J. and Xu, H. X., "Branched silver nanowires as controllable plasmon routers," Nano Lett. 10(5), 1950-1954 (2010).
[12] Wei, H., Wang, Z. X., Tian, X. R., Kall, M. and Xu, H. X., "Cascaded logic gates in nanophotonic plasmon networks," Nat. Commun. 2, 387 (2011).
[13] Wei, H., Li, Z. P, Tian, X. R, Wang, Z. X, Cong, F. Z, Liu, N., Zhang, S. P, Nordlander, P., Halas, N. J. and Xu, H. X., "Quantum dot-based local field imaging reveals plasmon-based interferometric logic in silver nanowire networks," Nano Lett. 11(2), 471-475 (2011).
[14] Mayer, K. M. and Hafner, J. H., "Localized surface plasmon resonance sensors," Chem. Rev. 111(6), 3828-3857 (2011).
[15] Wang, H., Wu, Y., Lassiter, B., Nehl, C. L., Hafner, J. H., Nordlander, P. and Halas, N. J., "Symmetry breaking in individual plasmonic nanoparticles," Proc. Natl. Acad. Sci. USA 103(29), 10856-10860 (2006).
[16] Zhang, Z., Weber-Bargioni, A., Wu, S. W., Dhuey, S., Cabrini, S. and Schuck, P. J., "Manipulating Nanoscale Light Fields with the Asymmetric Bowtie Nano-Colorsorter," Nano Lett. 9(12), 4505-4509 (2009).
[17] De Leon, I. and Berini, P., "Amplification of long-range surface plasmons by a dipolar gain medium," Nat. Photon. 4(6), 382-387 (2010).
[18] Gather, M. C., Meerholz, K., Danz, N. and Leosson, K., "Net optical gain in a plasmonic waveguide embedded in a fluorescent polymer," Nat. Photo. 4(7), 457-461 (2010).
[19] Kena-Cohen, S., Stavrinou, P. N., Bradley, D. D. and Maier, S. A., "Confined surface plasmon-polariton amplifiers," Nano Lett. 13(3), 1323-1329 (2013).
[20] Bolger, P. M., Dickson, W., Krasavin, A. V., Liebscher, L., Hickey, S. G., Skryabin, D. V. and Zayats, A. V., "Amplified spontaneous emission of surface plasmon polaritons and limitations on the increase of their propagation length," Opt. Lett. 35(8), 1197-1199 (2010).

[21] Oulton, R. F., Sorger, V. J., Genov, D. A., Pile, D. F. P. and Zhang, X., "A hybrid plasmonic waveguide for sub-wavelength confinement and long-range propagation," Nat. Photon. 2(8), 496-500 (2008).
[22] Wei, H., Zhang, S. P., Tian, X. R. and Xu, H. X., "Highly tunable propagating surface plasmons on supported silver nanowires," Proc. Natl. Acad. Sci. USA 110(12), 4494-4499 (2013).
[23] Pan, D., Wei, H., Jia, Z. L. and Xu, H. X., "Mode conversion of propagating surface plasmons in nanophotonic networks induced by structural symmetry breaking," Sci. Rep. 4, 4993 (2014).
[24] Bergman, D. J. and Stockman, M. I., "Surface plasmon amplification by stimulated emission of radiation: Quantum generation of coherent surface plasmons in nanosystems," Phys. Rev. Lett. 90(2), 027402 (2003).
[25] Berini, P. and De Leon, I., "Surface plasmon-polariton amplifiers and lasers," Nat. Photon. 6(1), 16-24 (2012).
[26] Liu, N., Wei, H., Li, J. P, Wang, Z. X, Tian, X. R, Pan, A. L. and Xu, H. X., "Plasmonic amplification with ultra-high optical gain at room temperature," Sci. Rep. 3, 1967 (2013).